cosmetics

MDPI

Article

Development and Characterization of 3D Senescent Models Mimicking Skin Aging

Loïc Pentecouteau, Céline Laperdrix *, Emeline Rouxel, Annick Folligné, Pierre-Yves Morvan and Romuald Vallée

Codif International, 61 Rue du Commandant l'Herminier, CS 51749, F-35417 Saint-Malo Cedex, France
* Correspondence: c.laperdrix@codif.com; Tel.: +33-(0)-2-23-18-31-31

Abstract: Aging, marked by a decline in cellular function and increased risk of diseases, involves the accumulation of senescent cells. This study aims to develop and characterize 3D senescent skin models to understand cellular senescence mechanisms' implications in cutaneous aging. Normal human epidermal keratinocytes (NHEKs) were cultured from early to late passages (p2 to p7) to induce replicative senescence or sourced from both young and aged donors to reconstruct 3D models. Histological analyses assessed tissue morphology and integrity, while permeability assays evaluated epidermal barrier function. Analyses using immunostaining, RT-PCR, Affymetrix™ GeneChip™ Microarrays identified key markers of cellular senescence, epidermal homeostasis, and other related processes. Results showed that NHEKs at p5 and beyond, and those from aged donors, exhibited significant morphological disruptions, decreased expression of differentiation-associated genes, and impaired barrier function. Increased p16ink4a-positive cells indicated enhanced senescence. Transcriptome analysis revealed significant changes in keratinocyte differentiation, cell–cell interaction, cell cycle regulation, extracellular matrix homeostasis, and inflammation. These findings underscore the relevance of addressing cellular senescence for enhancing skin health and promoting skin longevity. These 3D senescent skin models, validated by consistent results from both passage-induced senescence and aged donor keratinocytes, are valuable for understanding skin aging and developing anti-aging treatments, positioning them as essential tools in the pursuit of skin longevity-focused innovations.

Keywords: skin aging; skin longevity; cellular senescence; replicative senescence; tissue engineering; 3D skin models; epidermal differentiation

check for updates

Academic Editor: Enzo Berardesca

Received: 26 February 2025
Revised: 21 March 2025
Accepted: 27 March 2025
Published: 9 April 2025

Citation: Pentecouteau, L.; Laperdrix, C.; Rouxel, E.; Folligné, A.; Morvan, P.-Y.; Vallée, R. Development and Characterization of 3D Senescent Models Mimicking Skin Aging. *Cosmetics* **2025**, *12*, 71. https://doi.org/10.3390/cosmetics12020071

Copyright: © 2025 by the authors. Licensee MDPI, Basel, Switzerland. This article is an open access article distributed under the terms and conditions of the Creative Commons Attribution (CC BY) license (https://creativecommons.org/licenses/by/4.0/).

1. Introduction

Aging, traditionally defined as a 'Time-related dysfunction', is a complex process characterized by a gradual decline in cellular biological functions and an increased risk of age-related diseases [1]. As the global population ages, an increasing number of people are affected by this process. According to the World Health Organization (WHO) 2022, by 2030, one in six people worldwide will be 60 or older. By 2050, this percentage will rise to 22%, or 2.1 billion people. This demographic shift underscores the need for a deeper understanding of the biological mechanisms driving aging. Biologically, aging results from the cumulative impact of molecular and cellular damage over time.

Among these aging mechanisms, the accumulation of senescent cells stands out as particularly significant. Cellular senescence, often referred to as a state of 'irreversible growth arrest', occurs when cells lose their ability to divide but remain metabolically active. This process, while initially protective, contributes to tissue dysfunction over time. Originally described by Hayflick and Moorhead, replicative senescence is an irreversible

cell cycle arrest that typically occurs in cells after multiple culture passages, reflecting their limited proliferative capacity [2]. This state can be induced in response to various stimuli and plays roles in physiological processes such as development, cancer prevention, and cutaneous wound healing [3].

However, senescence also has a darker side, particularly in the context of aging, where the accumulation of these cells has been recognized as one of the 12 hallmarks of aging [4]. In addition to replicative senescence, primarily due to telomere shortening, cellular senescence can also be initiated by stress signals. These encompass oncogene-induced senescence (OIS), oxidative stress, mitochondrial dysfunction, or exposure to chemical compounds and ionizing radiations, as seen in therapy-induced senescence (TIS) [5,6].

Skin, as an interface between our environment and organism, is continually exposed to both internal and external stressors. Among these factors, chronic exposure to solar radiation, pollutants, and tobacco, collectively referred to as the skin aging exposome, are recognized as accelerators of extrinsic aging that potentiate intrinsic or chronological aging [7]. Senescent cell accumulation is observed in all compartments of the skin during aging, identified by increased senescence-associated β-galactosidase (SA-β-gal) activity or by other markers such as p16INK4a, p21CIP, and p53 [8–12]. At the level of the epidermis, Rübe et al. suggest the histone variant H2A.J as a new biomarker to detect senescent cells during human skin aging and show that in the epidermis, the proportions of H2A.J-expressing keratinocytes increased from ≈20% in young to ≈60% in aged skin [13]. Additionally, in the basal layer, an inverse correlation between Ki67+ and H2A.J+ keratinocytes was observed, which may be responsible for the decline in regenerative capacities of the epidermis and the slowing down of the skin healing process. Moreover, in addition to their accumulation, senescent cells secrete cytokines (IL-1, IL-6, IL-8), chemokines (GRO-α), growth factors (HGF, IGFBPs), and matrix metalloproteinases (MMP-3, MMP-1, MMP-9), collectively termed as senescence-associated secretory phenotype (SASP). SASP is thought to contribute to the functional decline of the skin as a consequence of aging, through the establishment of a chronic inflammatory state and induction of senescence in normal cells [14,15]. Interestingly, senescent fibroblasts in aged skin behave differently in vivo compared to in vitro. Waldera et al. demonstrated that intrinsically aged dermal fibroblasts develop a unique Skin Aging-Associated Secretory Proteome (SAASP), which is distinct from the classical SASP typically observed in vitro [16]. Keratinocytes play a critical role in maintaining epidermal integrity and regeneration. Their senescence not only disrupts the epidermal renewal process but also exacerbates inflammatory and degenerative processes associated with aging, making their unique behavior particularly relevant to skin aging studies. This highlights the limitations of traditional 2D models in fully replicating the complexity of the in vivo environment, reinforcing the need for 3D models that better mimic the cellular and extracellular context of aged skin, including the unique behaviors of senescent keratinocytes.

At the histological level, aged skin is characterized by a thinning epidermis, a flattened dermo–epidermal junction (DEJ), and dermal alterations, all attributable to senescent cell activity. These changes have motivated the development of innovative anti-aging therapies targeting senescent cells. Such therapies, including senomorphic agents, senolytics, and senostatics, aim to counteract SASP effects or selectively eliminate senescent cells. Emerging strategies also leverage the immune system to clear these cells [17].

To support the development of these innovative therapies and further our understanding of senescence mechanisms in a more physiologically representative context, we have developed and characterized 3D models of aged skin. These models, which mimic the cellular and microenvironmental complexity of aged skin more accurately than traditional

2D cultures or biochemical assays [18], offer invaluable tools for testing senotherapies and studying cellular senescence. They provide a critical understanding of the challenges and future directions of managing skin aging at the clinical level. This work opens the door to a deeper understanding of skin longevity and the development of more effective treatments for promoting long-term skin health and addressing age-related skin conditions.

2. Materials and Methods

2.1. Cell Cultures

Normal human epidermal keratinocytes (NHEKs) were derived from three donors aged 7 (isolated from foreskin), 27, and 50 years (isolated from abdominal plasty). The NHEK cells were cultured in keratinocyte serum-free medium (KSFM) supplemented with bovine pituitary extract (50 µg/mL) and epidermal growth factor (EGF) (5 µg/mL). To model differential aging processes, NHEK cells underwent multiple passages using trypsinization, followed by a 1:3 split, based on the methodology outlined by Hayflick [19]. The cells from passages 2 (p2) through 7 (p7) were used for epidermal reconstruction.

Normal human dermal fibroblasts (NHDF) were established from mammary plasty of healthy donors. These cells were obtained from a pool of five donors aged 21 to 51 years. The NHDF were cultured and amplified in calcium-free DMEM, which was then incorporated into a three-dimensional collagen lattice. This enriched matrix provided a scaffold for keratinocyte seeding, enabling the 3D reconstruction of human skin.

All procedures involving human cells were conducted in accordance with the ethical standards of the institutional and national research committees and with the 1964 Helsinki Declaration and its later amendments or comparable ethical standards.

2.2. Reconstructed Human Epidermis (RHE)

Reconstructed human epidermis (RHE) samples were prepared as previously described [20]. Briefly, suspensions of NHEKs from the 7-year-old donor at p2 to p7 were cultured on 0.5 cm^2 polycarbonate culture inserts (Millipore, Molsheim, France) in Epilife® medium (Invitrogen Life Technologies, Carlsbad, CA, USA) supplemented with Epilife® supplements and then transferred to the air–medium interface for 5 or 12 days and grown in Epilife® medium (Invitrogen Life Technologies, Carlsbad, CA, USA) supplemented with 1.5 mmol calcium chloride and 50 µg/mL ascorbic acid.

In parallel, RHEs were also prepared with NHEK from young and aged donors used at low passages. Specifically, NHEKs from the 7-year-old donor (p3) and the 27-year-old donor (p3) were utilized for these reconstructions. Depending on the model, RHEs were matured and cultured for 5 to 17 days, as indicated in the results section. After this period, RHEs were collected for histological, permeability, immunostaining, or gene expression analysis. All experimental conditions were performed in triplicate.

2.3. Reconstructed Human Skin (RHS)

Reconstructed human skin (RHS) samples were cultured using a well-established protocol for 3D skin models. Normal human epidermal keratinocytes (NHEKs), derived from a 7-year-old donor and ranging from passages 2 to 7, along with cells from both younger and older donors, specifically the 7-year-old and 50-year-old donors, were seeded on a three-dimensional collagen lattice. The lattice, containing fibroblasts and made from type I collagen (Advanced BioMatrix, Carlsbad, CA, USA), was cast in a 0.5 cm^2 culture insert (Millipore). The lattice was prepared using a medium consisting of MEM and complete Epilife® medium, supplemented with type I collagen, L-glutamine, and $NaHCO_3$.

After polymerization, keratinocytes were seeded onto the lattice and then incubated at 37 °C in a 5% CO_2 environment for 48 h using a seeding medium of Epilife® without IGF-1,

supplemented with insulin and $CaCl_2$. After the initial incubation period, the medium was removed, allowing the reconstructed skins to be maintained in air/liquid interface conditions. The differentiation test medium used during the cultivation period of 5 to 17 days was Epilife® without IGF-1, supplemented with insulin, $CaCl_2$, vitamin C, and keratinocyte growth factor (KGF). The medium under the inserts was changed every 2 or 3 days. After the cultivation periods, RHS samples were harvested for histological examination, immunostaining, and comprehensive genomic analysis using Affymetrix platforms (Santa Clara, CA, USA).

2.4. Histological and Immunostaining Analysis

The RHE and RHS samples were collected, washed, and fixed with formaldehyde solution. Fixed tissues were dehydrated with increasing ethanol concentrations and embedded in paraffin, and sections were carried out using a microtome (5 µm thickness). Next, the sections were deparaffinized, rehydrated, and stained with hematoxylin-eosin saffron (HES). Image acquisition of stained tissue sections was performed on a microscope at a Nikon ECLIPSE Ci-L microscope with a NIKON DS-Ri2 camera. Images were used to determine the morphological aspect of the RHE and thickness of the epidermis using NDP.view2 Viewing software V2.0.

Immunohistochemistry and immunofluorescence staining were performed for protein quantification in RHE or RHS. Samples were cut into 5 µm-thick sections, and stainings were performed using monoclonal antibodies against human p16ink4a (clone E6H4, 1:50, Roche Diagnostics, Meylan, France) or Ki67 (Rabbit monoclonal SP6, 1:200, Abcam, Cambridge, UK). Sections were observed using a Nikon ECLIPSE Ci-L. The images were captured using a NIKON DS-Ri2 and processed with Nikon NIS Elements software Ar V5.02.03. For quantitative analyses, the intensity of p16ink4a and Ki67 staining were measured in five representative areas for each section using ImageJ2 release 2.16.0 software (National Institute of Health, Bethesda, MA, USA) [21].

2.5. RHE Permeability Measurements

Skin barrier quality was assessed by measuring ^{14}C-caffeine penetration in the RHE constructed with NHEKs derived from a 7-year-old donor ranging from p2 to p7. ^{14}C-caffeine diluted in a water–alcohol-containing gel (80% water and 8% ethanol) was deposited on the surface of the RHE. To prevent evaporation, the tops of the cells were sealed with a cap. The receptor fluid, containing the absorbed radioactivity, was collected in scintillation vials at 30 min intervals over a period of 8 h (30 min, 1, 2, 3, 4, 5, 6, 7, and 8 h). The radioactivity was measured using a Tricarb Packard Coulter. Caffeine diffusion was inversely proportional to the barrier function, with higher permeability indicating a weaker barrier.

2.6. Total RNA Extraction and Quantitative RT-qPCR

Total RNA from RHE and RHS samples were isolated using the RNeasy Plus Mini Kit (Qiagen, Maryland, MD, USA). To evaluate the quantity and quality of the isolated total RNA, capillary electrophoresis was performed using the Bioanalyzer 2100 (Agilent Technologies, Santaclara, CA, USA) equipped with RNA Nano Chips (Agilent Technologies). The RNA samples were subsequently reverse transcribed using SuperScript II Reverse Transcriptase (Invitrogen Life Technologies, Carlsbad, CA, USA) following the manufacturer's instructions. Then, samples were amplified by RT-qPCR using PowerUp™ SYBR™ Green (Thermofisher, Waltham, MA, USA) and specific primer (CDKN2A forward and reverse sequence respectively: 5′-3′ ATATGCCTTCCCCCACTACC; 5′-3′ GCCATTTGCTAGCAGTGTGA; MKI67 forward and reverse sequence, respectively: 5′-3′ GACAGAGGTTCCTAAGAGAG; 5′-3′ AACAATCAGATTTGCTTCCG).

2.7. Differentially Expressed Genes

Comparative analysis of differentially expressed genes was performed on RHS samples, one reconstructed with NHEK cells from a 7-year-old donor at p2 and the other with NHEKs at p5, using the HG-U219 array (Affymetrix®). The Affymetrix platform was specifically used to identify genes between these passages whose expression levels changed by at least a two-fold (fold change). Total RNA was extracted from RHS samples using TriPure Isolation Reagent (Thermo Fisher Scientific, Waltham, MA, USA). The quality and concentration of the RNA were assessed with the Agilent 2100 Bioanalyzer system. An equal amount of high-quality RNA was used across samples to ensure uniformity in subsequent analyses. Biotinylated antisense RNA (aRNA) was synthesized from extracted RNA using the GeneChip 3′IVT Express Kit (Affymetrix). The integrity and size distribution of the aRNA were verified both pre- and post-fragmentation using the Bioanalyzer 2100. Fragmented aRNA samples were hybridized to the Affymetrix HG-U219 array, which assays over 36,000 transcripts. Hybridization occurred at 45 °C for 20 h using the GeneAtlas Fluidics Station (Affymetrix). Post-hybridization, arrays were scanned at a resolution of 2 µm by the GeneAtlas Imaging Station to acquire signal intensities. Acquired raw intensity data were processed using the Affymetrix Expression Console software. Background correction and normalization were performed using the Robust Multiarray Analysis (RMA) method, which includes log2 transformation and quantile normalization. Differentially expressed genes between samples from passage 2 (p2) and passage 5 (p5) NHEK cells were identified based on a minimum two-fold change criterion. Significantly modulated genes were uploaded to DAVID (Database for Annotation, Visualization, and Integrated Discovery, http://david.abcc.ncifcrf.gov/, accessed on 20 March 2025) for functional annotation. Pathway enrichment analysis, including access to Reactome pathways, was performed using DAVID's integrated tools [22].

2.8. Statistical Analysis

Data are presented as mean ± SEM. Statistical significance was determined using unpaired Student's *t*-test or one-way ANOVA with Dunnett's multiple comparisons. $p < 0.05$ was considered significant. * $p < 0.05$, ** $p < 0.01$, *** $p < 0.001$.

3. Results

3.1. Morphological Analysis of RHEs Constructed from NHEKs Subjected to Early to Late Passages

To appreciate the effects of varying passages of NHEKs on in vitro epidermal reconstruction, we cultivated these cells across a range of passages from 2 to 7 (p2 to p7). This approach was designed to approximate the Hayflick limit, thus simulating cellular senescence. As expected, histological analysis of the RHEs using NHEKs from these different passages revealed distinct morphological differences associated with the passage number. Specifically, RHE samples from early passages (p2 to p4) exhibited a normal epidermal morphology (Figure 1A–C). These models were distinguished by complete epidermal stratification observed with the four expected cell layers, indicative of the effective establishment of the terminal differentiation program in keratinocytes. However, with increasing passage numbers, significant morphological changes were observed (Figure 1D–F). RHEs constructed with NHEKs at p5 and p6 displayed a thinner epidermal layer, along with a disrupted differentiation program, evidenced by the presence of nuclei or parakeratosis in the cornified layer. The most pronounced alterations were observed in RHEs derived from NHEKs at p7. These samples showed marked disorganization, complete lack of stratification, and severe impairment in both the differentiation program and epidermal integrity.

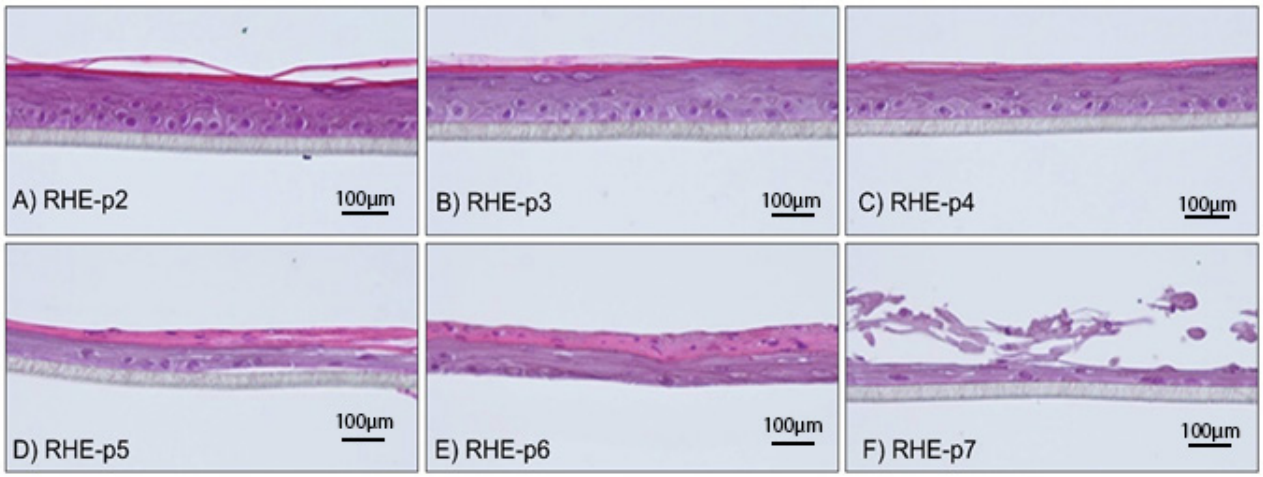


Figure 1. Histological analysis of reconstructed human epidermis (RHE) from normal human epidermal keratinocytes (NHEKs) at various passages. Hematoxylin and eosin staining was performed on RHE samples after 12 days of culture. (**A**–**C**) RHEs from early-passage NHEKs (RHE-p2 to RHE-p4) show normal morphology and complete stratification. (**D**–**F**) RHEs from late-passage NHEKs (RHE-p5 to RHE-p7) exhibit thinner layers and the presence of parakeratosis, demonstrating a disrupted epidermal terminal differentiation process.

3.2. Assessment of the Epidermal Barrier Function of the RHE-p2 to RHE-p7

The measurement of caffeine permeability was used to assess the integrity of the 'outside-in' epidermal barrier of RHEs constructed with NHEKs at p2 to p7 and cultured for either 5 or 12 days. As expected, RHEs developed from NHEKs at p2 to p4 exhibited a significantly lower permeability, indicating a functional epidermal barrier, in contrast to RHEs constructed using late-passage NHEKs (Figure 2). Thirty minutes after caffeine application, its permeability was about markedly lower in RHEs from NHEKs at p2 to p4 compared to RHEs from NHEKs at p5 to p7. However, it is noteworthy that RHEs cultured for 5 days displayed a similar caffeine penetration after 5 h, suggesting that the barrier was not fully functional at this early time point (Figure 2A). In contrast, by the 12th day of culture, RHEs generated from NHEKs at p2 to p4 appeared to exhibit a completely functional epidermal barrier demonstrated by a lower caffeine penetration, compared to RHEs made from NHEKs at p5 to p7 (Figure 2B).

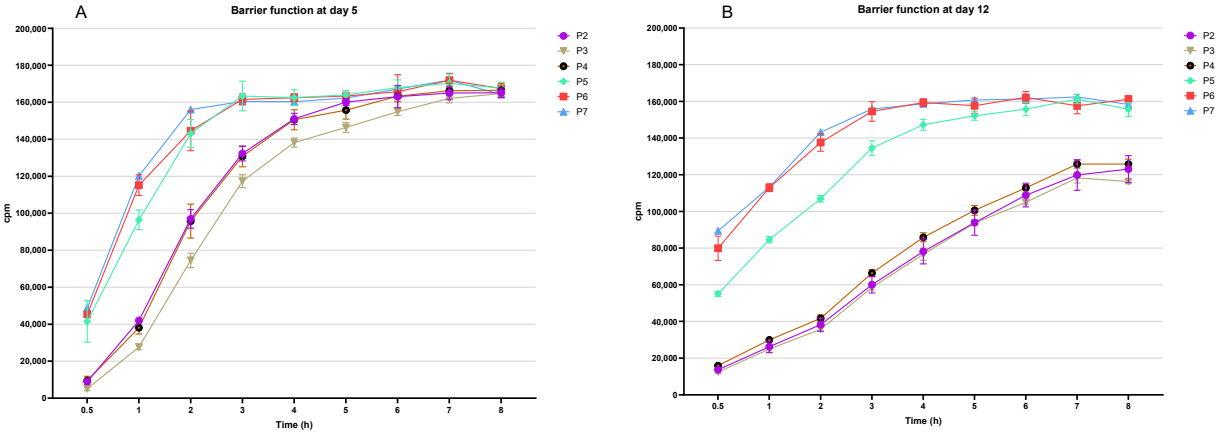


Figure 2. Assessment of the epidermal barrier function of reconstructed human epidermis (RHE) from normal human epidermal keratinocytes (NHEKs) at various passages. The permeability of

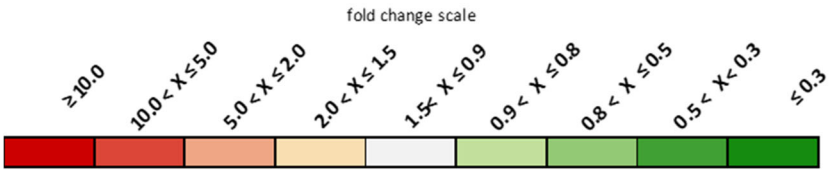
caffeine was measured to evaluate barrier integrity in RHEs constructed with NHEKs at passages 2 to 7, cultured for either 5 days (D5) (**A**) or 12 days (D12) (**B**). RHEs from early-passage NHEKs (p2 to p4) showed lower permeability, indicating a more functional barrier compared to those from late-passage NHEKs (p5 to p7), which exhibited higher permeability and compromised barrier function.

3.3. Analysis of Gene Expression of Epidermal Markers in RHE-p2 to RHE-p7

Gene expression analysis was performed to assess the impact of keratinocyte passage number on key markers of epidermal homeostasis. The results aligned with histological observations and permeability assessments, revealing a clear trend of decreased expression in markers related to keratinocyte differentiation, epidermal integrity, and barrier function in RHEs derived from late-passage NHEKs (p5 to p7). Specifically, genes encoding Keratin 1, filaggrin, caspase 14, calmodulin-like 5 (CALML5), corneodesmosin, and desmoglein 1—all essential for the maintenance of a functional epidermal barrier—showed a marked reduction in expression in these later-passage models (Table 1). This reduction points to a disruption in the epidermal differentiation program and weakened barrier function in late-passage RHEs.

Table 1. Gene expression analysis of key epidermal markers in reconstructed human epidermis (RHE) using normal human epidermal keratinocytes (NHEKs) at passages 2 to 7 (p2 to p7). Expression levels are presented as fold change relative values compared to a control, which corresponds to the epidermis constructed with keratinocytes at passage 1 (p1) and normalized by changes in glyceraldehyde-3-phosphate dehydrogenase (GAPDH) values, reflecting the changes associated with keratinocyte differentiation, maintenance of epidermal integrity, barrier function, and inflammation. The table highlights a decrease in the expression of differentiation markers and an increase in basal layer markers and pro-inflammatory genes in RHEs from late-passage NHEKs, indicating disrupted differentiation and barrier function.

	Genes		P2	P3	P4	P5	P6	P7
			Fold Change Versus p1					
	Calmodulin-like 5	CALML5	1.09	0.76	0.58	0.26	0.12	0.05
Keratinocyte differentiation	Caspase 14, apoptosis-related cysteine peptidase	CASP14	1.01	0.65	0.48	0.32	0.17	0.07
	Filaggrin	FLG	1.01	0.93	0.84	0.38	0.16	0.08
	Keratin 1	KRT1	0.96	0.58	0.58	0.33	0.23	0.20
	Keratin 19	KRT19	1.16	1.19	2.22	4.85	9.39	16.14
	Sulfotransferase family, cytosolic, 2B, member 1	SULT2B1	0.97	0.68	0.89	0.45	0.23	0.28
	Laminin, gamma 2	LAMC2	0.85	0.51	1.87	3.39	5.94	7.81
Glycerol/water transport	Aquaporin 3 (Gill blood group)	AQP3	1.17	0.73	0.82	0.76	0.42	0.42
Cytokines/Chemokines	Interleukin 1, alpha	IL1A	0.95	1.22	1.73	1.26	1.84	3.07
Anti-microbian peptides, innate immunity	Defensin, beta 4A	DEFB4A	0.65	0.81	2.86	0.09	0.02	0.01
	S100 calcium-binding protein A7	S100A7	0.87	1.10	6.04	3.76	0.75	1.25
Cell–cell interactions	Corneodesmosin	CDSN	0.82	0.76	0.74	0.38	0.12	0.14
	Desmoglein 1	DSG1	1.16	0.88	1.14	0.65	0.45	0.41



In contrast, markers associated with basal layer stemness or undifferentiated keratinocytes, such as Keratin 19 and Laminin Gamma 2 (LAMC2), were significantly upreg-

ulated in RHEs developed from higher passages. This increase in basal markers further suggests a disruption in the keratinocyte differentiation process, with late-passage keratinocytes failing to complete the transition into mature, differentiated cells [23].

The analysis of antimicrobial peptide (AMP) gene expression also revealed differences between early- and late-passage RHEs. Notably, S100A7 (psoriasin), a gene linked to disrupted epidermal differentiation and inflammation, was significantly upregulated in RHEs from NHEK at p4 and p5 (Table 1). This finding aligns with the impaired differentiation seen in other models of epidermal inflammation, such as psoriasis, suggesting that these passages may mimic early signs of stress or inflammatory conditions [24].

Interestingly, RHEs constructed from NHEK at p7 exhibited a significant increase in gene expression of IL-1α, suggesting a pro-inflammatory state that may be associated with altered epidermal integrity and barrier function. In senescent cells, IL-1 signaling is closely associated with the development of the senescence-associated secretory phenotype (SASP) [25], a secretory state characterized by the production of more than 40 factors involved in intercellular signaling [26]. This upregulation of IL-1α in late-passage keratinocytes likely reflects the pro-inflammatory environment typical of aging skin, where senescent cells accumulate and contribute to impaired epidermal function through SASP, further emphasizing the relevance of this model for studying the impact of aging on skin integrity.

3.4. Analysis of Senescent Cell Accumulation in RHE-p3 vs. RHE-p5

RHEs derived from NHEKs at p3 or p5, cultured for 5 or 10 days, and stained for p16Ink4a—a specific biomarker for senescence and aging—demonstrated a notable increase in p16Ink4a-positive keratinocytes and accompanying epidermal thinning as the NHEK passages increased. The proportion of senescent keratinocytes in RHEs from NHEK at p5 exhibited a 234% ($p < 0.001$) increase compared to those from p3, indicating a significant rise in senescence with the advancement of cell passages (Figure 3). In RHE-p7, p16Ink4a-positive keratinocytes are mainly detected in the basal layer.

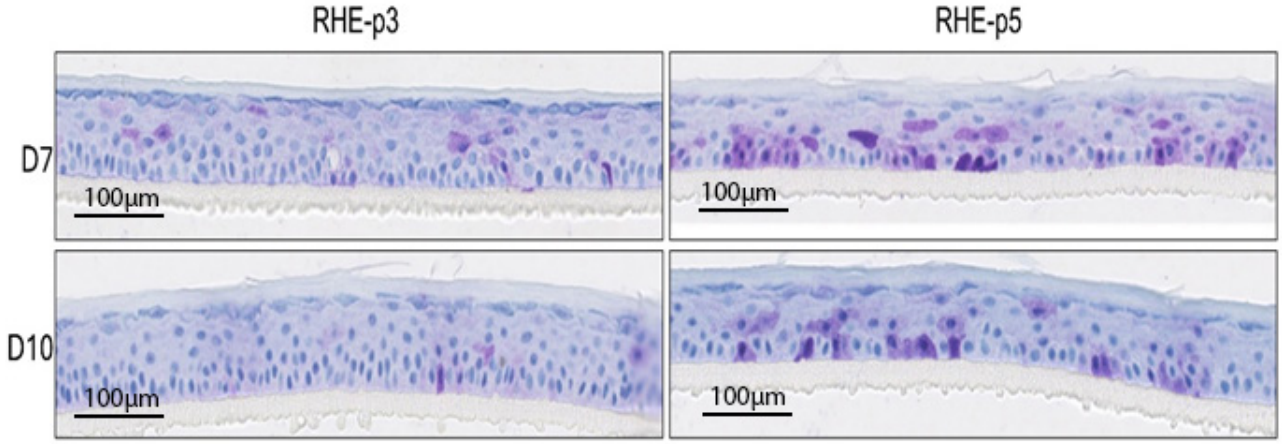


Figure 3. Histological sections of reconstructed human epidermis (RHE) from normal human epidermal keratinocytes (NHEK) at passage 3 (RHE-p3) and passage 5 (RHE-p5), after 7 days (D7) and 10 days (D10) of culture, stained for p16Ink4a to detect senescent cells.

3.5. Morphological Analysis of RHEs Constructed from NHEK Derived from Young and Aged Donors

After characterizing our model by using different passage numbers of keratinocytes to simulate the aging process in RHEs through senescent cell accumulation, we subsequently analyzed RHEs reconstructed from NHEK obtained from both young (RHE-Young) and aged (RHE-Old) donors. In both cases, the RHEs exhibited complete stratification with

different basal and suprabasal layers, as well as the formation of a cornified layer (Figure 4). However, RHEs reconstructed with aged keratinocytes demonstrated significant thinning compared to those reconstructed with young cells, either after 10 or 17 days of culture.

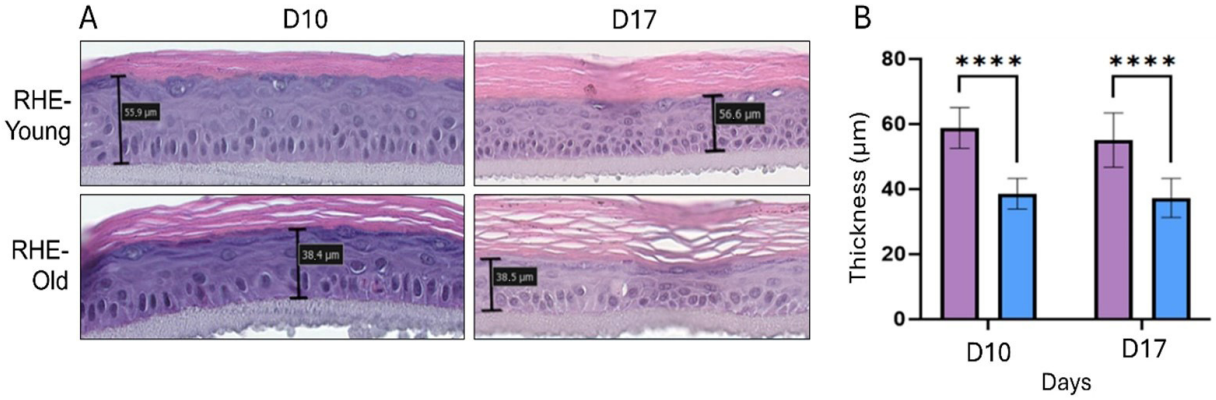


Figure 4. (**A**) Hematoxylin-eosin saffron stain and morphological analysis of reconstructed human epidermis (RHE) from normal human epidermal keratinocytes (NHEKz) derived from young (RHE-Young) and aged (RHE-Old) donors after 10 days (D10) and 17 days (J17) of culture. (**B**) Quantification of the average epidermal thickness between RHE-Young (pink) and RHE-Old (blue) at 10 days and 17 days of culture. A significant reduction in thickness is observed in RHEs from aged NHEKs compared to those from young NHEKs at both time points (**** $p < 0.0001$).

3.6. Analysis of Proliferation and Senescent Markers in RHE-Young vs. RHE-Old

RT-qPCR analyses indicated significant upregulation of the CDKN2A gene, which encodes for the senescence marker p16Ink4a, in RHEs reconstructed from aged NHEKs, observed either after both 10 and 17 days of culture (Figure 5A). Conversely, the MIKI67 gene, related to cell proliferation, showed enhanced expression in aged RHEs compared to young after 10 days. However, by day 17, young NHEK-derived RHEs demonstrated greater MIKI67 expression. Protein-level analysis mirrored these trends, with p16 more prevalent in aged RHEs initially, whereas, by day 17, the proliferation indicator ki67 was predominantly observed in young RHEs (Figure 5B).

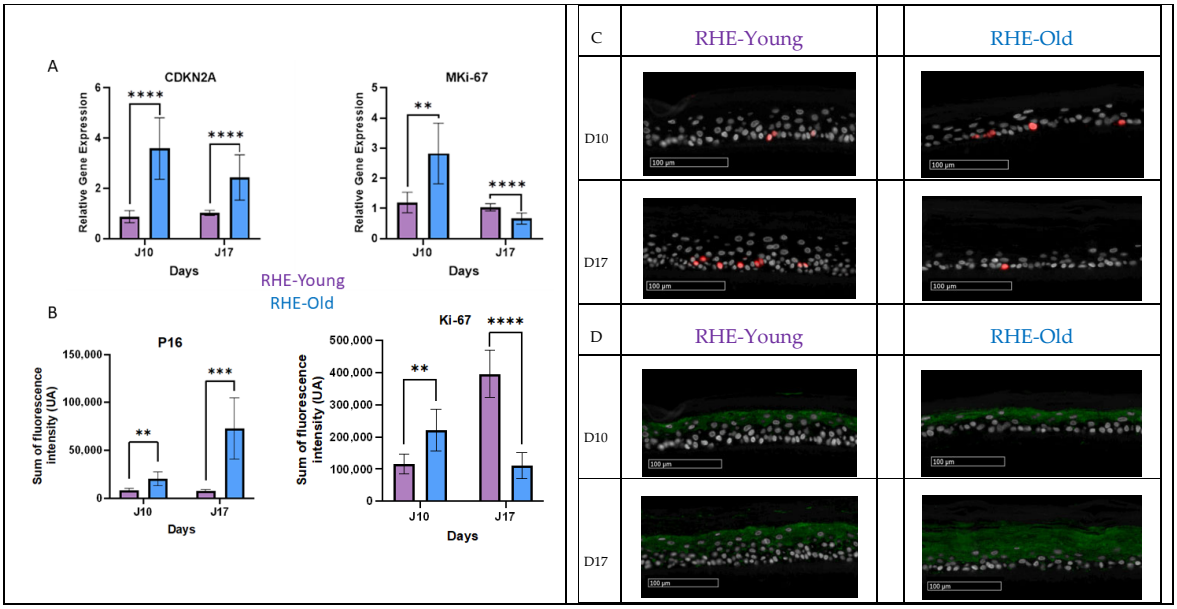


Figure 5. Analysis of proliferation and senescence markers in reconstructed human epidermis (RHE) from young (RHE-Young) and aged (RHE-Old) normal human epidermal keratinocytes (NHEK) after

10 days (J10) and 17 days (J17) of culture. (**A**) RT-qPCR analysis of the relative expression of CDKN2A (left) and MKI67 (right) genes in RHE-Young and RHE-Old at J10 and J17 of culture. (**B**) Protein-level analysis showing the quantification of p16 (left) and Ki67 (right) protein expression in RHE-Young and RHE-Old at J10 and J17 of culture (** $p < 0.01$; *** $p < 0.001$; **** $p < 0.0001$). (**C**) RHE section, Ki67 (red) DNA labels (grey) (**D**) RHE section, P16 (green) DNA labels (Grey). *IMF* analysis of proliferation (**A**) and senescence (**B**) markers in reconstructed human epidermis (RHE) from young (RHE-Young) and aged (RHE-Old) normal human epidermal keratinocytes (NHEKs) after 10 days (J10) and 17 days (J17) of culture.

3.7. Morphological Analysis of RHS Constructed from NHEKs Subjected to Early to Late Passages

To further characterize our model and approach the complexity of skin physiology and aging, we reconstructed human full-thickness models using NHEKs at various passages. Unsurprisingly, the morphologies of the epidermises from skin models reconstructed with late-passage NHEK (RHS-p5 and RHS-p7) showed serious alterations, unlike the epidermises reconstructed with NHEK at p2 (RHS-p2) (Figure 6A–C). Similar to the RHE models, an alteration in the differentiation program was observed, characterized by the presence of nuclei or parakeratosis in the nucleus, a loss of integrity in the living layers indicated by a loss of keratinocyte adhesion, and a significant alteration in the cohesion between the epidermis and the dermal equivalent.

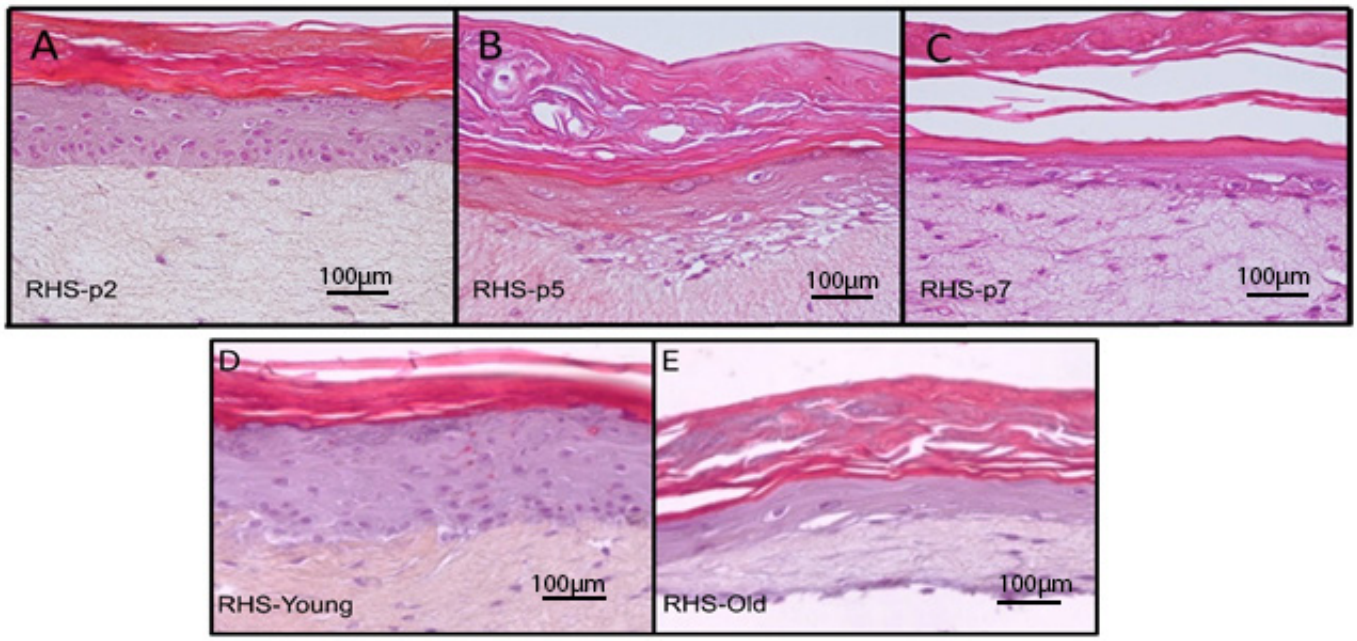


Figure 6. Morphological analysis of reconstructed human skin (RHS) from normal human epidermal keratinocytes (NHEKs) at different passages (**A**–**C**) and from young and aged donors (**D**,**E**). (**A**–**C**) Histological sections of RHS with NHEKs at various passages: (**A**) RHS-p2 with normal morphology, (**B**) RHS-p5 with altered morphology and parakeratosis, and (**C**) RHS-p7 with significant disorganization and loss of integrity. (**D**,**E**) Histological sections of RHS with NHEKs from young and aged donors: (**D**) RHS-Young with well-structured epidermis, and (**E**) RHS-Old with thinned epidermis and disorganization.

3.8. Morphological Analysis of RHS Constructed from NHEKs Derived from Young and Aged Donors

The reconstructed skins with aged keratinocytes (RHS-Old) showed altered morphology, similar to models made with late-passage NHEK, including a thinned epidermis, parakeratosis, and disorganization of the various living layers of the epidermis (Figure 6D,E). Young keratinocytes enabled the reconstruction of a complete epidermis (RHS-Young),

including the various layers, with a granular layer characterized by the presence of keratohyalin granules, suggesting the correct terminal differentiation program of keratinocytes.

3.9. Differential Gene Expression in RHS-p5 Versus RHS-p2

After conducting a histological characterization and analyzing senescence markers in our models, gene expression profiling using Affymetrix Human Genome U219 Array was performed on RNA isolated from RHS-p5 and compared to RNA isolated from RHS-p2, both cultured for 14 days. This analysis revealed 1281 differential gene expression, identifying 636 genes upregulated (fold change FC > 2; $p < 0.05$) and 645 genes downregulated (fold change FC < 0.5; $p < 0.05$) in RHS-p5 compared to RHS-p2. A comprehensive list of all differentially expressed genes with at least a two-fold change, including upregulated and downregulated genes, is provided in Supplemental Data S1.

Subsequent bioinformatic analysis of these differentially expressed genes highlighted that the most significantly enriched Gene Ontology (GO) terms are directly associated with key biological processes such as keratinocyte differentiation (Table 2) (e.g., KRT2, KRT4, KRT13, KRT19, KRT75, KRT77, SPRR3, SPRR4, RPTN, LCE5A, TCHH, CRNN, ELF5), cell–cell interaction (e.g., ITGAM, DSC), cell cycle regulation (e.g., CDKN2A, CCND1, CCNB2, CDK1, CDKN3, MKI67), matrix synthesis and degradation (e.g., MMP7), and inflammation (e.g., CCL5, VEGFA).

Table 2. Differential gene expression in RHS reconstructed from NHEK p5 versus p2.

Gene Title	Gene Symbol	Fold Change	Function Related to Skin
Keratinocyte Differentiation			
Keratin 13	KRT13	11.07	Structure of intermediate filaments in epithelial cells
Keratin 19	KRT19	8.4	
Keratin 77	KRT77	7.82	
Keratin 75	KRT75	7.07	
Keratin 4	KRT4	4.87	
Keratin 2	KRT2	4.75	
Small proline-rich protein 4	SPRR4	11.63	Epidermal barrier
Small proline-rich protein 3	SPRR3	5.17	
Repetin	RPTN	5.36	
Late cornified envelope 5A	LCE5A	6.18	
Trichohyalin	TCHH	15.65	
Cornulin	CRNN	8.58	
E74-like factor 5 (ets domain transcription factor)	ELF5	9.72	
Cell–Cell Interaction			
Integrin, alpha M (complement component 3 receptor 3 subunit)	ITGAM	8.73	Cell adhesion and immune response
Cell Cycle Regulation			
Cyclin-dependent kinase inhibitor 2A	CDKN2A	3.36	Regulation of cell cycle and cellular senescence
Cyclin D1	CCND1	3.12	Regulation of cell cycle
Cyclin B2	CCNB2	0.33	
Cyclin-dependent kinase 1	CDK1	0.27	
Cyclin-dependent kinase inhibitor 3	CDKN3	0.2	
Matrix Synthesis and Degradation			
Matrix metallopeptidase 7 (matrilysin, uterine)	MMP7	0.1	Extracellular matrix degradation and tissue remodeling
Inflammation			
Chemokine (C-C motif) ligand 5	CCL5	0.28	Modulation of immune response
Vascular endothelial growth factor A	VEGFA	0.4	Regulation of angiogenesis and vascular permeability
Additional Key Processes (Senescence, Growth Arrest, Apoptosis Resistance)			
Sestrin 3	SESN3	2.9	Regulation of oxidative stress and cellular signaling
Cellular retinoic acid binding protein 2	CRABP2	3.04	Regulation of retinoic acid activity
Protein phosphatase 1, regulatory (inhibitor) subunit 1C	PPP1R1C	3.59	Regulation of cellular signaling
Apolipoprotein E	APOE	6.7	Lipid transport and tissue repair
Kallikrein-related peptidase 6	KLK6	6.31	Proteolysis and modulation of skin desquamation
Kallikrein 1	KLK1	4.47	

Table 2. *Cont.*

Gene Title	Gene Symbol	Fold Change	Function Related to Skin
Triggering receptor expressed on myeloid cells 2	TREM2	6.85	Modulation of immune response
Chloride channel accessory 4	CLCA4	11.67	Regulation of chloride ion transport and ionic homeostasis
Parathyroid hormone-like hormone	PTHLH	10.18	Regulation of cell growth and development
Alcohol dehydrogenase 7 (class IV), mu or sigma polypeptide	ADH7	10.8	Metabolism of retinoids and alcohol
Fetuin B	FETUB	10.51	Inhibition of pathological calcification and regulation of cell proliferation
Galanin prepropeptide	GAL	3.22	Regulation of inflammation and cellular stress response

The functional annotation of differentially expressed genes using the DAVID Bioinformatics Resources provided valuable insights into enriched Reactome Pathways, revealing that 69.6% of these genes were mapped to specific molecular pathways. Among the most significantly enriched pathways, those related to cell cycle regulation, mitotic checkpoints, and DNA replication stood out, reflecting the profound impact of senescence-induced dysregulation on keratinocyte homeostasis (Supplemental Data S2).

Pathways such as cell cycle progression, DNA synthesis, and mitotic phase checkpoints displayed high levels of enrichment, underlining the critical role of senescence in disrupting normal epidermal renewal processes. Furthermore, pathways linked to extracellular matrix formation and organization underscored the broader functional impairments observed in RHS-p5 models, demonstrating how the senescence phenotype extends beyond the epidermis to affect dermal homeostasis.

Notably, a number of genes differentially expressed between RHS-p5 and RHS-p2 play key functions in cellular processes such as senescence, growth arrest, and apoptosis resistance, including CCDN2, CDKN2A, CCND1, MKI67, and CDK1. Additionally, genes such as DSC2, CERS3, STMN1, KRT15, DCS3, TGM3, and TP63 were significantly downregulated (fold change FC < 0.5; $p < 0.05$) in RHS-p5 compared to RHS-p2, potentially contributing to the alteration of the differentiation program and barrier function (Table 2).

4. Discussion

A significant challenge within the cosmetic industry lies in the development of active ingredients that not only combat visible signs of aging but also promote skin longevity by targeting underlying biological mechanisms. Establishing the efficacy of these ingredients is essential, necessitating the adoption of 3D models that closely replicate the specific skin conditions. These advanced 3D models not only provide a more accurate representation of the skin's microenvironment in response to anti-aging compounds but also offer a critical step towards ensuring the safety and effectiveness of these ingredients before proceeding to clinical trials.

Our findings align with the fact that skin aging is marked by the reduction in proliferation and the accumulation of senescent cells, validated respectively by the decrease of Ki67 [11,13] and the increased presence of p16INK4a-positive cells [27,28]. Senescent cells contribute to tissue microenvironment deterioration through the secretion of the SASP, which has been widely reported to promote ongoing chronic, low-grade inflammation [12–29]. Consequently, these cells have emerged as key targets for therapeutic strategies, utilizing active ingredients that exhibit either senolytic properties, aiming to eliminate senescent cells, or senomorphic properties, seeking to modulate the harmful effects of the SASP. This perspective aligns with previously discussed evidence on cellular senescence in skin aging, demonstrating the potential of senotherapeutics to improve skin longevity and appearance [30].

To date, numerous models have been developed in an effort to closely mimic not only normal skin but also various skin processes or diseases, including photoaging or extrinsic aging, wound healing, psoriasis, atopic dermatitis, and even skin cancers [31,32]. However, models specifically replicating chronological aging through keratinocyte senescence have been lacking. While fibroblast-based senescence models have been used, such as those generated by continuous culture until growth arrest or through oxidative stress [32–34], the absence of keratinocyte-specific models leaves a gap in understanding the epidermal aging process. By addressing this limitation, our keratinocyte-based replicative senescence models provide a unique and complementary tool to existing photoaging and disease-specific models.

In our research, we focused on establishing a reliable 3D model of keratinocyte senescence. To achieve this, we employed the concept of replicative senescence, also referred to as the Hayflick limit, as a means to replicate passage number-induced replicative senescence [2]. By adopting this method, we significantly minimized the impact of genetic variability that could potentially influence the intrinsic aging process. This represents a significant advancement compared to earlier models that simply contrasted RHEs prepared from keratinocytes of young and elderly donors [35]. Building on previous research, our findings reinforce the model's validity by confirming an elevation in the p16INK4A level, a key indicator of cellular aging and senescent cell accumulation, in RHEs derived both from aged keratinocytes and those exposed to replicative senescence.

Interestingly, in our model of RHEs made from NHEK at p3 and p5, it appears that senescent keratinocytes are predominantly located in the basal layer, aligning with observations that the proliferative capacity of basal keratinocytes decreases with age, leading to epidermal thinning. Moreover, this observation is supported by our findings in RHE models derived from aged keratinocytes, which reveal an inverse correlation between Ki67+ (a marker of cell proliferation) and p16INK4A levels after 17 days of culture. Similarly, an inverse relationship was observed between Ki67-expression and histone variant H2A.J staining in germinative layers of skin biopsies isolated from young and old donors [13].

The maintenance of epidermal homeostasis requires a delicate balance between the proliferation and differentiation of keratinocytes. Therefore, in RHE-p2 to RHE-p7, the progression from normal to altered morphology with increasing passage number clearly illustrates the senescence-associated decline in epidermal integrity and function. The accumulation of senescent cells leads to alterations in the regenerative capacity of keratinocyte progenitors, resulting in a disrupted keratinocyte differentiation program and barrier function. These effects were observed in our study, particularly evident with the increase in caffeine penetration in RHEs made with late-passage NHEKs. Furthermore, significant changes in gene expression related to epidermal differentiation were identified, highlighting the molecular underpinnings of the observed phenotypic changes. These findings collectively illuminate the deleterious effects of senescence on the epidermal barrier and provide insight into the molecular dynamics that drive the decline in epidermal health with age.

To further characterize our model of reconstructed skin utilizing normal human epidermal keratinocytes (NHEKs) at either early (p2) or late (p5) stages, we compared the transcriptomes of RHS-p2 and RHS-p5. These comparisons demonstrated significant changes in gene expression, especially among genes linked to keratinocyte differentiation. Specifically, we observed modulation in late-stage markers involved in cornified envelope formation, such as the "fused" gene family within the epidermal differentiation complex on chromosome 1q21, including genes like SPRR3, SPRR4, and CRNN, which codes for cornulin. Notably, the gene modulation observed in our model reflects the trend toward senescence and validates the relevance of our 3D model in simulating chronological epi-

dermal aging. Additionally, gene expression changes were observed in pathways related to cell cycle regulation, DNA replication, and cell cycle checkpoints. These pathways are clearly influenced by the passage number, as the senescence of keratinocytes progressively disrupts their proliferation and differentiation processes. Furthermore, ECM-related pathways demonstrated that senescent keratinocytes also affect the dermal compartment, highlighting the relevance of our RHS model that integrates multiple skin compartments, illustrating how senescence in keratinocytes can influence other cellular layers, such as fibroblasts and the extracellular matrix.

For this type of protocol, as for every study using human donors, it is very important to collect as much information as possible. The goal is to limit interindividual variations and to obtain confident validation of donors. Age is necessary, and the anatomic site could also be considered, as photoaging may impact the results. But the genetic heritage of people could induce uncoherent results as well. That is why, before each experiment, validation of the number of passages was checked and validated to obtain real variations in senescence markers. To be more concrete, it is necessary to pre-select the donors in order to validate them and obtain a significant difference between the so-called young donor and the donor or the passage mimicking a donor, allowing the reconstruction of a senescent 3D model.

5. Conclusions

Our work contributes significantly to the broader efforts in anti-aging research, emphasizing the critical need to target cellular senescence for developing effective skin longevity-focused innovations. This study presents the successful development and characterization of 3D in vitro senescent skin models to mimic skin aging. By using normal human epidermal keratinocytes (NHEKs) from early to late passages and from both young and aged donors, we validated these models through histological analyses, permeability assays, and assessments of senescence markers. Our findings demonstrate significant morphological disruptions and impaired barrier functions in NHEK at passage 5 and beyond, as well as in those from aged donors.

These results demonstrate the challenges of reproducibility associated with NHEK passaging while highlighting the effectiveness of early passage keratinocytes from both young and aged donors in constructing reliable senescent models. This approach provides a solid foundation for understanding the mechanisms of skin aging and developing targeted treatments.

Additionally, as the trend in skincare increasingly focuses on promoting skin longevity, our research shows the importance of addressing cellular senescence to support long-term skin resilience, health, and appearance. Future studies should prioritize the identification and validation of senolytic, senostatic, or senomorphic agents to counteract the undesirable effects of aging, aligning with innovations aimed at enhancing skin longevity-focused solutions.

Supplementary Materials: The following supporting information can be downloaded at: https://www.mdpi.com/article/10.3390/cosmetics12020071/s1, Data S1: Genes identified by microarray analysis as having at least two-fold altered expression between RHS-p5 and RHS-p2. Data S2: of differentially expressed genes using DAVID Bioinformatics Resources and Reactome Pathways.

Author Contributions: L.P., P.-Y.M. and R.V. conducted the methodology, E.R. and A.F. conducted the data analysis. C.L. wrote the manuscript. L.P., E.R. and A.F. participated in the methodology. All authors have read and agreed to the published version of the manuscript.

Funding: CODIF funded this research.

Institutional Review Board Statement: Not applicable.

Informed Consent Statement: The cells used in this study were obtained from informed donors who provided written consent and conform to the ethical standards of the institutional and national research committees and with the 1964 Helsinki Declaration and its later amendments or comparable ethical standards.

Data Availability Statement: The data presented in this study are available upon request from the corresponding author. The data are not publicly available due to privacy restrictions.

Acknowledgments: We would like to thank the company QIMA Life Sciences for its precious help with the results, and Alain Deguercy, ex-BIO-Alternatives COO, for his invaluable technical guidance and support throughout this project. We also extend our gratitude to the H2P2 platform for providing the necessary technical resources and expertise. Special thanks go to Rachida Nachat-Kappes for her assistance with the preparation and writing of this manuscript.

Conflicts of Interest: Authors are all employed by the company Codif International. The authors declare that the research was conducted in the absence of any commercial or financial relationships that could be construed as a potential conflict of interest. The authors declare that this study received funding from CODIF. The funder was not involved in the study design, collection, analysis, interpretation of data, the writing of this article or the decision to submit it for publication.

References

1. Kyriazis, M. Aging as "Time-Related Dysfunction": A Perspective. *Front. Med.* **2020**, *7*, 371. [CrossRef] [PubMed]
2. Hayflick, L.; Moorhead, P.S. The serial cultivation of human diploid cell strains. *Exp. Cell Res.* **1961**, *25*, 585–621. [CrossRef] [PubMed]
3. Andrade, A.M.; Sun, M.; Gasek, N.S.; Hargis, G.R.; Sharafieh, R.; Xu, M. Role of Senescent Cells in Cutaneous Wound Healing. *Biology* **2022**, *11*, 1731. [CrossRef] [PubMed]
4. López-Otín, C.; Blasco, M.A.; Partridge, L.; Serrano, M.; Kroemer, G. Hallmarks of aging: An expanding universe. *Cell* **2023**, *186*, 243–278. [CrossRef]
5. Zhu, M.J.; Wang, X.; Shi, L.; Liang, L.Y.; Wang, Y. Senescence, oxidative stress and mitochondria dysfunction. *Med. Res. Innov.* **2018**, *21*, 24. [CrossRef]
6. Kim, J.H.; Brown, S.L.; Gordon, M.N. Radiation-induced senescence: Therapeutic opportunities. *Radiat. Oncol.* **2023**, *18*, 10. [CrossRef]
7. Krutmann, J.; Bouloc, A.; Sore, G.; Bernard, B.A.; Passeron, T. The skin aging exposome. *J. Dermatol. Sci.* **2017**, *85*, 152–161. [CrossRef]
8. Hickson, L.J.; Langhi Prata, L.G.P.; Bobart, S.A.; Evans, T.K.; Giorgadze, N.; Hashmi, S.K.; Herrmann, S.M.; Jensen, M.D.; Jia, Q.; Jordan, K.L.; et al. Senolytics decrease senescent cells in humans: Preliminary report from a clinical trial of Dasatinib plus Quercetin in individuals with diabetic kidney disease. *EBioMedicine* **2019**, *47*, 446–456. [CrossRef]
9. Victorelli, S.; Lagnado, A.; Halim, J.; Moore, W.; Talbot, D.; Barrett, K.; Chapman, J.; Birch, J.; Ogrodnik, M.; Meves, A.; et al. Senescent human melanocytes drive skin ageing via paracrine telomere dysfunction. *EMBO J.* **2019**, *38*, e101982. [CrossRef]
10. Ressler, S.; Bartkova, J.; Niederegger, H.; Bartek, J.; Scharffetter-Kochanek, K.; Jansen-Dürr, P.; Wlaschek, M. p16INK4A is a robust in vivo biomarker of cellular aging in human skin. *Aging Cell* **2006**, *5*, 379–389. [CrossRef]
11. Ogrodnik, M.; Acosta, J.C.; Adams, P.D.; d'Adda di Fagagna, F.; Baker, D.J.; Bishop, C.L.; Chandra, T.; Collado, M.; Gil, J.; Gorgoulis, V.; et al. Guidelines for minimal information on cellular senescence experimentation in vivo. *Cell* **2024**, *187*, 4150–4175. [CrossRef]
12. Ho, C.Y.; Dreesen, O. Faces of cellular senescence in skin aging. *Mech. Ageing Dev.* **2021**, *198*, 111525. [CrossRef]
13. Rübe, C.E.; Bäumert, C.; Schuler, N.; Isermann, A.; Schmal, Z.; Glanemann, M.; Mann, C.; Scherthan, H. Human skin aging is associated with increased expression of the histone variant H2A.J in the epidermis. *NPJ Aging Mech. Dis.* **2021**, *7*, 7. [CrossRef] [PubMed]
14. Ghosh, K.; Capell, B.C. The Senescence-Associated Secretory Phenotype: Critical Effector in Skin Cancer and Aging. *J. Investig. Dermatol.* **2016**, *136*, 2133–2139. [CrossRef]
15. Coppé, J.P.; Patil, C.K.; Rodier, F.; Sun, Y.; Muñoz, D.P.; Goldstein, J.; Nelson, P.S.; Desprez, P.-Y.; Campisi, J. Senescence-Associated Secretory Phenotypes Reveal Cell-Nonautonomous Functions of Oncogenic RAS and the p53 Tumor Suppressor. *PLoS Biol.* **2008**, *6*, e301. [CrossRef]
16. Waldera Lupa, D.M.; Kalfalah, F.; Safferling, K.; Boukamp, P.; Poschmann, G.; Volpi, E.; Götz-Rösch, C.; Bernerd, F.; Haag, L.; Huebenthal, U.; et al. Characterization of Skin Aging–Associated Secreted Proteins (SAASP) Produced by Dermal Fibroblasts Isolated from Intrinsically Aged Human Skin. *J. Investig. Dermatol.* **2015**, *135*, 1954–1968. [CrossRef] [PubMed]

17. Song, P.; An, J.; Zou, M.H. Immune Clearance of Senescent Cells to Combat Ageing and Chronic Diseases. *Cells* **2020**, *9*, 671. [CrossRef] [PubMed]
18. Cruz, A.M.; Gonçalves, M.C.; Marques, M.S.; Veiga, F.; Paiva-Santos, A.C.; Pires, P.C. In Vitro Models for Anti-Aging Efficacy Assessment: A Critical Update in Dermocosmetic Research. *Cosmetics* **2023**, *10*, 66. [CrossRef]
19. Hayflick, L. The limited in vitro lifetime of human diploid cell strains. *Exp. Cell Res.* **1965**, *37*, 614–636. [CrossRef]
20. Guenou, H.; Nissan, X.; Larcher, F.; Feteira, J.; Lemaitre, G.; Saidani, M.; Del Rio, M.; Barrault, C.C.; Bernard, F.-X.; Peschanski, M.; et al. Human embryonic stem-cell derivatives for full reconstruction of the pluristratified epidermis: A preclinical study. *Lancet* **2009**, *374*, 1745–1753. [CrossRef]
21. Schneider, C.A.; Rasband, W.S.; Eliceiri, K.W. NIH Image to ImageJ: 25 years of image analysis. *Nat. Methods* **2012**, *9*, 671–675. [CrossRef]
22. Huang, D.W.; Sherman, B.T.; Lempicki, R.A. Systematic and integrative analysis of large gene lists using DAVID bioinformatics resources. *Nat. Protoc.* **2009**, *4*, 44–57. [CrossRef]
23. Gkegkes, I.D.; Aroni, K.; Agrogiannis, G.; Patsouris, E.S.; Konstantinidou, A.E. Expression of caspase-14 and keratin-19 in the human epidermis and appendages during fetal skin development. *Arch. Dermatol. Res.* **2013**, *305*, 379–387. [CrossRef]
24. Ekman, A.K.; Vegfors, J.; Eding, C.B.; Enerbäck, C. Overexpression of Psoriasin (S100A7) Contributes to Dysregulated Differentiation in Psoriasis. *Acta Derm.-Venereol.* **2017**, *97*, 441–448. [CrossRef]
25. Lau, L.; Porciuncula, A.; Yu, A.; Iwakura, Y.; David, G. Uncoupling the Senescence-Associated Secretory Phenotype from Cell Cycle Exit via Interleukin-1 Inactivation Unveils Its Protumorigenic Role. *Mol. Cell. Biol.* **2019**, *39*, e00586-18. [CrossRef] [PubMed]
26. Davalos, A.R.; Coppe, J.P.; Campisi, J.; Desprez, P.Y. Senescent cells as a source of inflammatory factors for tumor progression. *Cancer Metastasis Rev.* **2010**, *29*, 273. [CrossRef] [PubMed]
27. Waaijer, M.E.C.; Gunn, D.A.; Adams, P.D.; Pawlikowski, J.S.; Griffiths, C.E.M.; van Heemst, D.; Slagboom, P.E.; Westendorp, R.G.J.; Maier, A.B. P16INK4a Positive Cells in Human Skin Are Indicative of Local Elastic Fiber Morphology, Facial Wrinkling, and Perceived Age. *J. Gerontol. Ser. A Biomed. Sci. Med. Sci.* **2016**, *71*, 1022–1028. [CrossRef] [PubMed]
28. Dimri, G.P.; Lee, X.; Basile, G.; Acosta, M.; Scott, G.; Roskelley, C.; Medrano, E.E.; Linskens, M.; Rubelj, I.; Pereira-Smith, O.; et al. A biomarker that identifies senescent human cells in culture and in aging skin in vivo. *Proc. Natl. Acad. Sci. USA* **1995**, *92*, 9363–9367. [CrossRef]
29. Coppé, J.P.; Desprez, P.Y.; Krtolica, A.; Campisi, J. The Senescence-Associated Secretory Phenotype: The Dark Side of Tumor Suppression. *Annu. Rev. Pathol.* **2010**, *5*, 99–118. [CrossRef]
30. Wyles, S.P.; Carruthers, J.D.; Dashti, P.; Yu, G.; Yap, J.Q.; Gingery, A.; Tchkonia, T.; Kirkland, J. Cellular Senescence in Human Skin Aging: Leveraging Senotherapeutics. *Gerontology* **2023**, *70*, 7–14. [CrossRef]
31. Ahn, M.; Cho, W.-W.; Park, W.; Lee, J.-S.; Choi, M.-J.; Gao, Q.; Gao, G.; Cho, D.-W.; Kim, B.S. 3D biofabrication of diseased human skin models in vitro. *Biomater. Res.* **2023**, *27*, 80. [CrossRef] [PubMed]
32. Weinmüllner, R.; Zbiral, B.; Becirovic, A.; Stelzer, E.M.; Nagelreiter, F.; Schosserer, M.; Lämmermann, I.; Liendl, L.; Lang, M.; Terlecki-Zaniewicz, L.; et al. Organotypic human skin culture models constructed with senescent fibroblasts show hallmarks of skin aging. *NPJ Aging Mech. Dis.* **2020**, *6*, 4. [CrossRef] [PubMed]
33. Galvis, D.; Walsh, D.; Harries, L.W.; Latorre, E.; Rankin, J. A dynamical systems model for the measurement of cellular senescence. *J. R. Soc. Interface* **2019**, *16*, 20190311. [CrossRef]
34. Tigges, J.; Krutmann, J.; Fritsche, E.; Haendeler, J.; Schaal, H.; Fischer, J.W.; Kalfalah, F.; Reinke, H.; Reifenberger, G.; Stühler, K. The hallmarks of fibroblast ageing. *Mech. Ageing Dev.* **2014**, *138*, 26–44.
35. Adamus, J.; Aho, S.; Meldrum, H.; Bosko, C.; Lee, J.M. p16INK4A Influences the Aging Phenotype in the Living Skin Equivalent. *J. Invest. Dermatol.* **2014**, *134*, 1131–1133. [CrossRef] [PubMed]

Disclaimer/Publisher's Note: The statements, opinions and data contained in all publications are solely those of the individual author(s) and contributor(s) and not of MDPI and/or the editor(s). MDPI and/or the editor(s) disclaim responsibility for any injury to people or property resulting from any ideas, methods, instructions or products referred to in the content.